communications physics

ARTICLE

https://doi.org/10.1038/s42005-022-01120-w OPEN

All-fiber optical nonreciprocity based on parity-time-symmetric Fabry-Perot resonators

Zheng Li[1], Jiejun Zhang[1✉], Yanyan Zhi[1], Lingzhi Li[1], Baoliang Liao[1] & Jianping Yao[1,2✉]

Nonreciprocal light transmission in an all-fiber platform is critical in modern optical communication systems, which can avoid the packaging and integration process required in current devices based on magneto-optical or nonlinear materials. Here we propose and demonstrate an all-fiber device with remotely tunable isolation ratio and switchable isolation direction by constructing two mutually coupled Fabry-Perot (FP) resonators with identical geometry and balanced gain and loss. By controlling the pumping power, strong optical nonreciprocity is achieved due to gain saturation nonlinearity that is enhanced by the broken parity-time symmetry. Nonreciprocal light transmission with an isolation ratio of 8.58 dB at 1550 nm and an insertion loss of 2.5 dB is demonstrated. The isolation bandwidth is 125 MHz, which is determined by the bandwidths of the two coupled FP resonators. The proposed approach provides an all-fiber solution for a remotely tunable and optically controlled isolator, which may find applications in software-defined optical networks.

[1] Guangdong Provincial Key Laboratory of Optical Fiber Sensing and Communications, Institute of Photonics Technology, Jinan University, Guangzhou, China. [2] Microwave Photonics Research Laboratory, School of Electrical Engineering and Computer Science, University of Ottawa, Ottawa, ON, Canada. ✉email: zhangjiejun@jnu.edu.cn; jpyao@uottawa.ca

Optical nonreciprocity is of fundamental importance for signal processing in modern optical communication systems[1]. Nonreciprocal devices, such as optical isolators[1] and circulators[2,3], are widely used to implement routing in optical networks and to remove back reflections at optical interfaces[4]. To date, several techniques have been proposed to realize optical nonreciprocity, including magneto-optic effects[5–13], temporal modulation[14–18] and optical nonlinearity[19–35]. The most widely used technique to realize optical isolators is based on magneto-optic effects[5–9]. However, on-chip integration of magneto-optical materials is still challenging on a COMS-compatible platform. In addition, an isolator implemented based on the magneto-optic effects requires a strong external magnetic field, which may harmfully interface with adjacent optical elements and affect their functionalities. Temporal modulation is regarded as a promising solution to realize on-chip isolation, but strong modulation is usually needed which makes the device have high energy consumption[16–18]. Optical nonlinear process such as thermo-optic effect[19], nonlinear parametric amplification[20], Raman amplification[21], stimulated Brillouin scattering (SBS)[22–25], Kerr nonlinearities[26,27], optomechanical interactions[28–33], and gain/absorption saturation[34,35] were also used to achieve nonreciprocal transmission. However, those approaches usually require specially designed waveguides with strong optical nonlinearities to effectively exploit optical nonreciprocity, again making the device have high energy consumption.

The nonreciprocal devices reported in[16–35] are implemented on on-chip platforms, which can find applications in optical networks, especially on-chip photonic networks. For example, an integrated circulator implemented based on a spatially modified III-V quantum-well system can be used in an on-chip photonic network[3]. However, the employment of integrated isolators in an optical fiber network may not be an optimal solution due to the large loss resulted from the fiber to chip interfaces. All-fiber isolators, thanks to the inherent fiber nature, can be more conveniently employed in optical networks with much smaller insertion loss and better simplicity for deployment. The all-fiber isolators proposed in[12,13] were implemented based on magneto-optic effect, which requires a strong magnetic field, making the miniaturization of the devices challenging. Thus, magnetic-free all fiber isolators can be more attractive.

Parity-time (PT) symmetric systems are open non-Hermitian systems with balanced gain and loss configurations[36,37], which have been demonstrated on various physical platforms, including electronic[38], acoustic[39–44] and photonic platforms[45–51]. In particular, photonics has been proven to be a powerful platform to implement PT-symmetry or more general non-Hermitian systems due to the easiness in manipulating the gain, loss and refractive index of an optical waveguide, leading to the observation of many phenomena that are generally difficult or impossible to achieve in traditional systems, including loss-induced transparency[46], unidirectional invisibility[47,48], mode selection for single-mode lasing[49–51], and nonreciprocal transmission[34,35]. In a PT-symmetric system, optical nonlinearity can be strongly enhanced due to the highly confined localized eigenmodes. For example, the gain saturation effect can be exploited using PT symmetry to achieve nonreciprocal light transmission based on photonic integrated components, such as two directly coupled microtoroidal whispering gallery mode resonators (WGMRs)[34,35], which provides a promising solution for on-chip isolators.

In this paper, we propose an approach to implement nonreciprocal light transmission in an all-fiber device with remotely tunable isolation ratio and switchable isolation direction. Three cascaded fiber Bragg gratings (FBGs) are inscribed in an erbium-ytterbium co-doped fiber (EYDF) to form two mutually coupled Fabry-Perot (FP) resonators. The two FP resonators have an identical geometry with identical resonance wavelengths. The gain and loss of the FP resonators are manipulated by controlling the pumping power to make the device work in the PT symmetry breaking regime. Thanks to the PT symmetry, the eigenmodes in the resonators are strongly localized, which would strongly increase the gain saturation, making nonreciprocal light transmission significantly enhanced. Different from the previous demonstrations, the proposed all-fiber isolator, with a remotely switchable isolation direction, a tunable isolation ratio and a tunable bandwidth, can find potential applications in future software-defined reconfigurable optical interconnect networks.

Results and discussion

Operation principle. Figure 1a shows the schematic of the proposed all-fiber isolator. It consists of three uniform FBGs (FBG1, FBG2, and FBG3) inscribed in a short and erbium-ytterbium co-doped fiber (EYDF) to form two FP resonators (FP1 and FP2). The FP resonators are geometrically identical (i.e., FBG1 and FBG3 are identical, the lengths of FP1 and FP2 are the same, and FBG2 is a symmetrical FBG) and are mutually coupled, which ensures the degeneracy of the localized resonance frequencies. The net gain and loss in FP2 and FP1 can be tuned by controlling the pumping power and the pumping direction into the EYDF. If the pumping power is launched into the EYDF from the right side (the FP2 side), the pumping power in FP2 will be higher than that in FP1 due to the absorption along the EYDF. By controlling the pumping power, a net gain and loss can be achieved for FP2 and FP1, respectively. To achieve a high gain to loss ratio between FP2 and FP1, one can make the middle FBG (FBG2) have an additional reflection band at 980 nm to enable FP2 have more gain, or, in our case, apply a bending to the FP1 to make FP1 have higher loss. The details of the PT-symmetric FP resonators and their optical characteristics are discussed in detail in Supplementary Note 1.

Figure 1b shows the transmission spectrum of an individual FBG inscribed in a standard single-mode fiber (SMF). The FBG is used for spectrum measurement and estimation of the reflection coefficients and bandwidths of those three FBGs in the PT-symmetric FP resonators. As can be seen, the FBG has 3-dB bandwidth of 0.2 nm, a reflection of 12 dB. Figure 1c shows the spectrums of the isolator when operating in the unbroken PT-symmetric regime (top) and in the broken PT-symmetric regime (bottom). Within the reflection bandwidth of the FBGs, the two coupled resonators support four resonance modes. The mode spacing is 0.067 nm, corresponding to an effective cavity length of 12.4 mm. The resonance wavelength mismatch between FP1 and FP2 is removed by applying a strain to FP1 to compensate for the fabrication error that results in a cavity length difference between FP1 and FP2 (see Supplementary Note 2). Degeneracy of the eigenmodes of FP1 and FP2 is then realized. The operation of the system involves the coupling between the forward and backward light waves in both FP1 and FP2 resonators. The coupled differential equations can be written as

$$\begin{cases} \frac{da_1}{dt} = (i\Delta\omega_1 - \gamma)a_1 - i\mu a_2 + \sqrt{\kappa}\varepsilon_{\text{in}} \\ \frac{da_2}{dt} = (i\Delta\omega_2 + g_a)a_2 - i\mu a_1 \end{cases} \quad \begin{cases} \frac{db_1}{dt} = (i\Delta\omega_1 - \gamma)b_1 - i\mu b_2 \\ \frac{db_2}{dt} = (i\Delta\omega_2 + g_b)b_2 - i\mu b_1 + \sqrt{\kappa}\varepsilon_{\text{in}} \end{cases} \tag{1}$$

where a_1 and a_2 are the amplitudes of the forward light waves in FP1 and FP2, respectively; b_1 and b_2 are amplitudes of the backward light waves in FP1 and FP2, respectively; ω_1 and $\omega_2$are the local resonance frequencies of FP1 and FP2, respectively, μ is the coupling coefficient between FP1 and FP2 determined by the

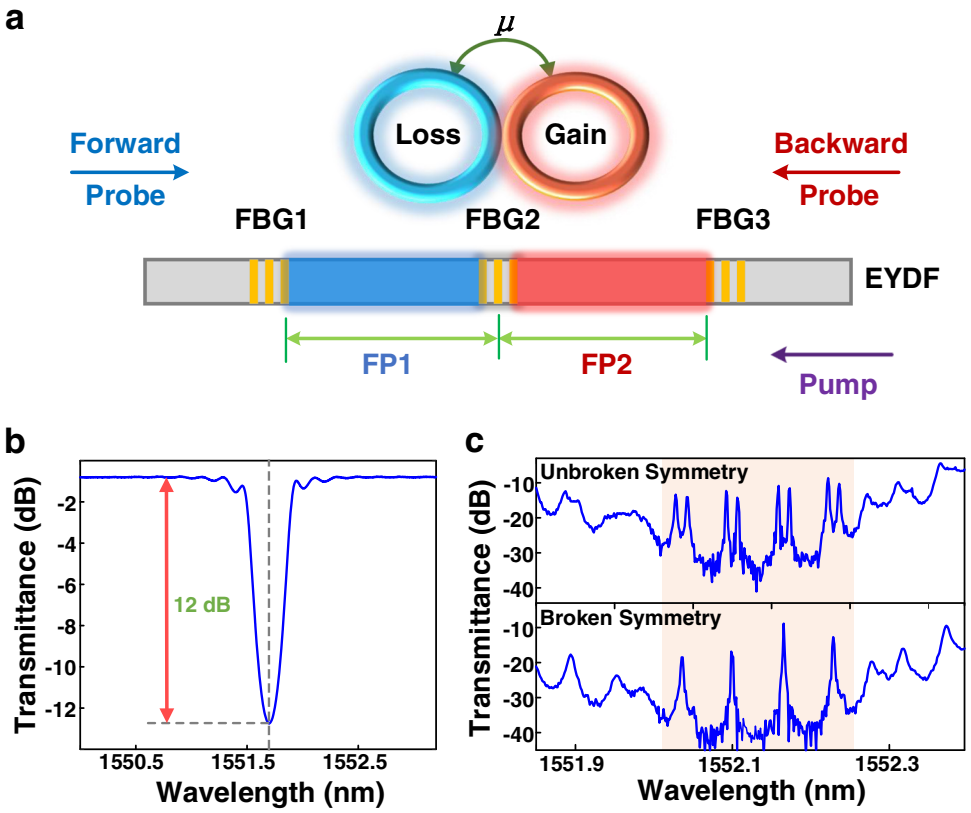

Fig. 1 Design of the all-fiber optical nonreciprocity. a Schematic of the PT-symmetric FP resonators for nonreciprocal transmission of light. FP1 and FP2 are the two resonators with FP1 having a loss and FP2 a gain. Based on the probe input directions, forward and backward propagation configurations are denoted by blue and red arrows, respectively. The purple arrow denotes the pump input direction. **b** Measured transmission spectrum of an individual FBG with identical fabrication parameters as those three in the PT-symmetric FP resonators. **c** Measured transmission spectra of the device in the unbroken PT-symmetric regime (top) and in the broken PT-symmetric regime (bottom). Resonances are observed in the reflection band (shaded brown) of the FBGs. FBG: fiber Bragg grating; EYDF: erbium-ytterbium co-doped fiber; FP: Fabry-Perot interferometer; PT: parity-time.

transmission coefficient of FBG2, $|\varepsilon_{\rm in}|^2$ is the power of the input signal, and $\Delta\omega_1 = \omega_0 - \omega_1$ and $\Delta\omega_2 = \omega_0 - \omega_2$ are the frequency detuning of the input optical signal from the local resonance frequencies of FP1 and FP2, respectively. The net gain of FP2 for forward and backward propagating probe lights are given by $g_{a,b} = g'/2 - \gamma_0/2 - \kappa/2$, where κ is the external coupling coefficient determined by the transmission coefficients of FBG1 and FBG3, and γ_0 is the intrinsic loss of the resonator. The nonlinearly saturated gain in an FP resonator is given by[52]

$$g' = \frac{g_0[1-(1+2|\mathbf{E}|^2/\mathbf{E}_{\rm s}^2)^{-1/2}]}{|\mathbf{E}|^2/\mathbf{E}_{\rm s}^2} \quad (2)$$

where g_0 is the small-signal gain coefficient of FP2, $\mathbf{E}$ is the electric field of the forward ($|\mathbf{E}| = a_2$) or backward ($|\mathbf{E}| = b_2$) transmission light in FP2, $\mathbf{E}_{\rm s}$ is the saturation electric field, and γ is the total loss of FP1.

By solving Eq. (1) in the steady-state approximation, the transmittance of the system, which is the power ratio between output and input intensities for both directions, are given by

$$T_{\rm f} = \left|\frac{S_{\rm out}^{\rm f}}{\varepsilon_{\rm in}}\right|^2 = \frac{\mu^2\kappa^2}{(-\Delta^2+\mu^2-g_a\gamma)^2+\Delta^2(g_a-\gamma)}$$
$$T_{\rm b} = \left|\frac{S_{\rm out}^{\rm b}}{\varepsilon_{\rm in}}\right|^2 = \frac{\mu^2\kappa^2}{(-\Delta^2+\mu^2-g_b\gamma)^2+\Delta^2(g_b-\gamma)} \quad (3)$$

where $|S_{\rm out}^{\rm f}|^2$ and $|S_{\rm out}^{\rm b}|^2$ are the output powers of the system when the input signal is launched in the forward and backward directions, respectively. We have $T_{\rm f} \neq T_{\rm b}$ when $g_a \neq g_b$, and the nonreciprocal light transmission can thus be achieved. To quantify the isolation performance of the system, we define a nonreciprocal isolation as $\eta = 10\times\log_{10}(T_{\rm f}/T_{\rm b})$, where $T_{\rm f}$ and $T_{\rm b}$ are the peak transmittivities of the forward and backward transmission spectra, respectively.

For a device with two mutually coupled PT-symmetric FP resonators, optical nonreciprocity is possible since the strong field localization in the gain FP resonator in the broken PT-symmetric regime enables the system to satisfy $g_a \neq g_b$. For an optical signal injected into the device from the gain FP resonator side, it will first experience gain saturation and then a loss in the loss FP resonator, while for an optical signal injected into the device from the loss FP resonator side, it will not experience gain saturation in the gain section, since the signal is very weak due to the loss in the loss section. Thus, an optical signal for forward and backward inputs will have unequal gains, resulting in nonreciprocity of light transmission in the device.

Experimental setup. Figure 2a illustrates the experimental setup to characterize the optical nonreciprocity of the device. The device is fabricated with three cascaded FBGs in an EYDF to form two mutually coupled FP resonators. The three FBGs have an identical length of 4 mm and a reflectivity of 12 dB. The physical spacing between two FBGs is 10 mm, as shown in Fig. 2b. An optical vector analyzer (OVA) is used to generate a wavelength-sweeping probe light which is applied to the device to measure its transmission spectrum. A 980-nm laser source is used to pump the EYDF. The polarizations of the probe and pump light waves are adjusted by two polarization controllers (PC1 and PC2), respectively. A gain-variable erbium-doped fiber amplifier (EDFA) is used to tune the power of the probe

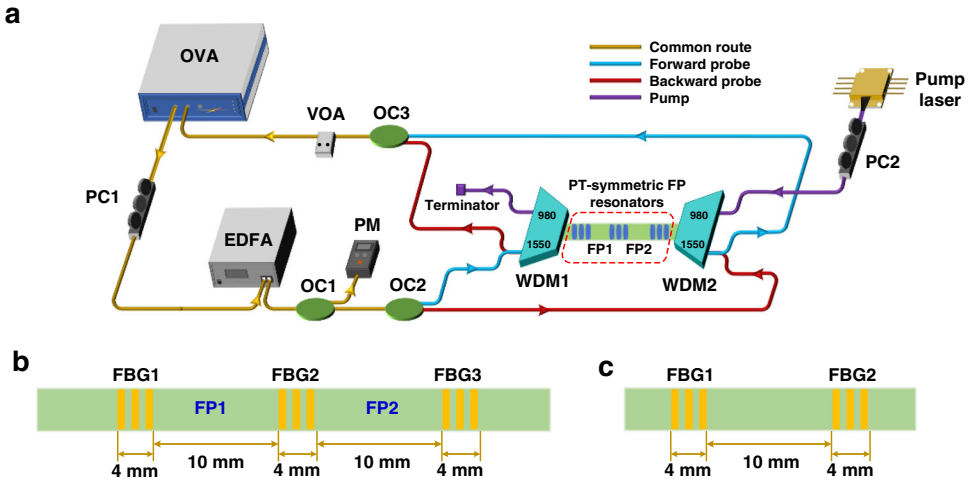

Fig. 2 Experimental setup. a Schematic of the experimental setup for forward and backward transmission measurements. Optical paths for forward and backward transmission are shown by the blue and red lines, respectively. The shared optical paths for both forward and backward transmission are shown by the yellow lines. The optical path for the pump light is shown by the purple line. **b** A fabricated all-fiber nonreciprocal device based on parity-time-symmetric FP resonators. **c** A fabricated single FP resonator on an EYDF to characterize the gain-saturation nonlinearity in the FP resonator. OVA: optical vector analyzer; VOA: variable optical attenuator; PC: polarization controller; EDFA: erbium-doped fiber amplifier; OC: optical coupler; PM: power meter; WDM: wavelength division multiplexer; FBG: fiber Bragg grating; PT: parity-time; FP: Fabry-Perot interferometer; EYDF: erbium-ytterbium co-doped fiber.

light launched into the device, with its output power being monitored in real time using a power meter (PM) via an optical coupler (OC1). For forward light transmission measurements, the probe light goes through OC2 and is launched into the device through the 1550-nm port of a wavelength division multiplexer (WDM1). After passing through FP1 and FP2, the probe light is obtained at the output of the device through the 1550-nm port of a second WDM (WDM2). The transmitted probe light goes through OC3 and is detected at the OVA after being attenuated at a variable optical attenuator. For backward light transmission measurements, the probe light goes into the device through the 1550-nm port of WDM2. After passing through FP2 and FP1, the probe light is obtained at the output of the device through the 1550-nm port of WDM1. In both measurements, the pump light is launched into the device from the 980-nm port of WDM2, and the residual pump light is terminated at a terminator connected to the 980-nm port of WDM1.

Characterization of gain and nonlinearity. First, we investigate the gain saturation behavior of a single FP resonator. To do so, an FP resonator consisting of two FBGs with an identical length of 4 mm and a reflectivity of 12 dB is fabricated in an EYDF. The two FBGs are placed with a physical spacing of 10 mm, as shown in Fig. 2c. We first measure the output power when the input probe power is fixed at −15 dBm while increasing the 980-nm pumping power from 0 to 200 mW. As can be seen from Fig. 3a, a maximum gain is achieved when the pumping power is 100 mW. Further increasing pumping power will not increase the gain. Then, we fix the pumping power at 100 mW while increasing the probe power from −15 to 10 dBm. As shown in Fig. 3b, when the probe power is less than −10 dBm, we have the highest gain. Further increasing the probe power will lead to gain saturation. The results indicate that the gain saturation can be achieved by choosing a proper pumping power and a proper probe power. For a single FP resonator, optical nonreciprocity is not possible since an optical signal, injected into the cavity from either direction, will be trapped in the cavity and will experience the same gain.

Measurements of optical nonreciprocity. Next, the optical nonreciprocity of the proposed all-fiber device consisting of two mutually coupled FP resonators is experimentally evaluated. To do so, we fabricate three cascaded FBGs in an EYDF to form two mutually coupled FP resonators. The three FBGs have an identical length of 4 mm and a reflectivity of 12 dB. The physical spacing between two adjacent FBGs is 10 mm, as shown in Fig. 2c. The device is partially mounted on a micro-positioning platform, which allows stretching only FP1, so that the lengths of the two resonators can be controlled to match accurately. The tuning process is shown in detail in Fig. S3. To obtain nonreciprocal transmission, the system should work in the PT-symmetric broken regime. In the experiment, the gain is introduced to FP2 by optically pumping the EYDF. The system become PT-symmetric by adjusting the pumping power to balance the gain/loss ratio between the two coupled FP resonators (i.e., $g = \gamma$). With a balanced gain/loss ratio, the system is in the broken PT-symmetric regime when $\mu < \gamma$, and the eigenfrequencies share the same real parts but complementary imaginary parts. In this case, the transmission spectrum of the device is similar to that of a single FP resonator, with a single transmission peak at each resonance wavelength of FP1 or FP2, as shown in Fig. 1c. The transmission peak corresponds to two degenerate eigenmodes of the PT-symmetric FP resonators, with a gain mode having a positive imaginary part and a loss mode having a negative imaginary part. The gain mode is strongly confined in the gain resonator FP2[49], thus enhancing the gain saturation to allow optical nonreciprocity with a high isolation ratio. As shown in Fig. 4a, the transmittances at the eigenfrequency of the PT-symmetric FP resonators for the forward and backward lights are measured to be 0.13 and 0.02, respectively, corresponding to an isolation ratio of $\eta = 8.58$ dB with the pumping power of 100 mW for an input probe power of 0 dBm.

We also investigate the operation of the device when operating in the PT-symmetric unbroken regime. At the same input probe power of 0 dBm, the pumping power and the bending loss of the FP1 are reduced such that the magnitude of the gain and loss coefficients is smaller than that of the coupling coefficient, or $\mu > \gamma$. Mode splitting is observed in the transmission spectrum, as shown in Fig. 4b. Due to the weak eigenmode localization[49], the nonreciprocal transmission is only a result of gain saturation of the EYDF without the enhancement by the PT symmetric modes. The transmittances of the

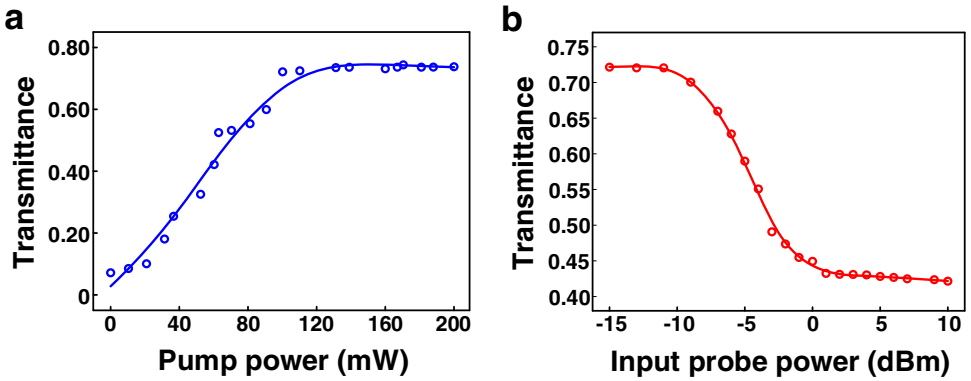

Fig. 3 Gain saturation response. Gain saturation response of a single FP resonator shown in Fig. 2c, **a** with a fixed probe power of -15 dBm, and **b** with a fixed pumping power of 100 mW. The effective mode field diameter of the fiber is 6.9 μm.

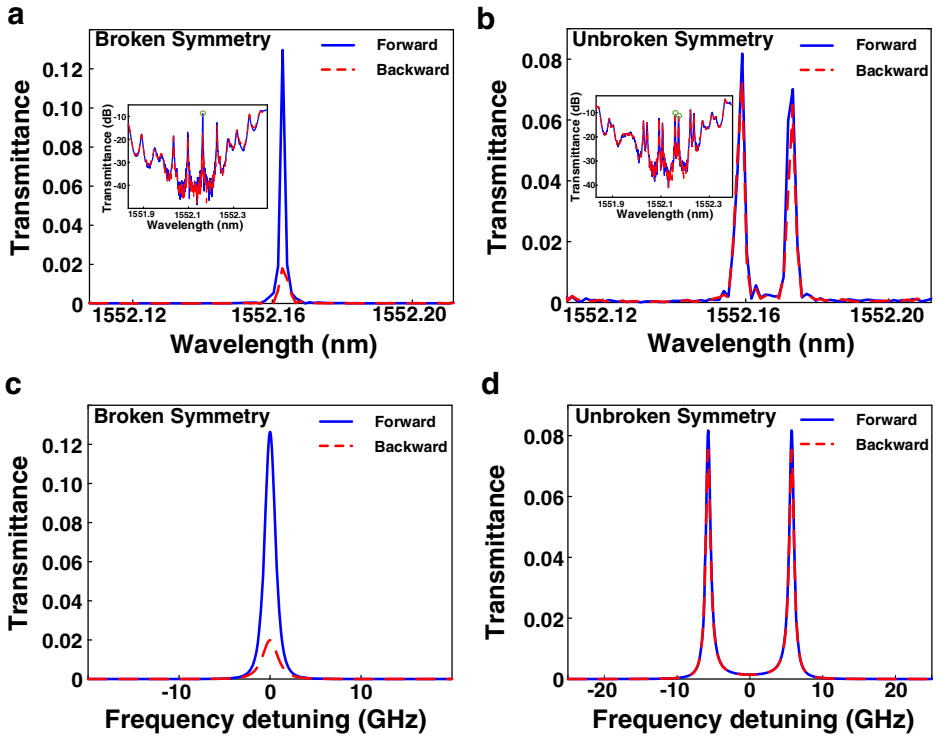

Fig. 4 Nonreciprocal light transmission. Experimental results of nonreciprocal light transmission of the device in **a** the broken PT-symmetric regime, and **b** in the unbroken PT-symmetric regime. Inset: the total transmission spectrum of the device in a logarithmic scale. **c** and **d**, Simulation results corresponding to those in **a** and **b**.

nondegenerate eigenmodes are measured to have similar values for both forward and backward light waves. Figure 4c and d shows the simulated results, showing a good agreement with those experimentally measured results. The details on light transmission in the PT-symmetric FP resonators with broken and unbroken symmetries are discussed in Supplementary Note 3.

Performance of the nonreciprocal device. The performance of the device is compared with the optical nonreciprocal devices previously reported based on different schemes in Table 1 in Supplementary Note 4. Specifically, the total insertion loss of the proposed device is measured to be 2.5 dB, which is resulted from a fiber splice loss of 0.4 dB from the two fusion joints between the EYDF and the SMF, a gain of 0.28 dB provided by the pumped EYDF for the entire device, and a loss of 2.38 dB from the coupled FP resonators due to the mismatch between the reflectivities of the three FBGs. The total insertion loss of the device is 2.5 dB, which can still be reduced with an improved fabrication technique, especially by eliminating the mismatch of the reflectivities. Note that the power consumption of 100 mW refers to the output power of the pump laser, which is not the pumping power absorbed in the PT-symmetric FP resonators. The actual power consumption of the device is estimated to be less than 32.97 mW. The details for the estimation of the power consumption of the device are provided in Supplementary Note 5.

To further study the nonreciprocity performance, a simulation is performed in which the parameters are optimized. The result shows that, by optimizing the design of the FP resonators and utilizing active fibers with better amplification performance, an isolation ratio of 33 dB or an operation bandwidth of over 56 GHz can be achieved for different application requirements (See Supplementary Note 6).

Since the optical nonreciprocity is resulted from an enhanced gain saturation in the PT-symmetric FP resonators, it is dependent

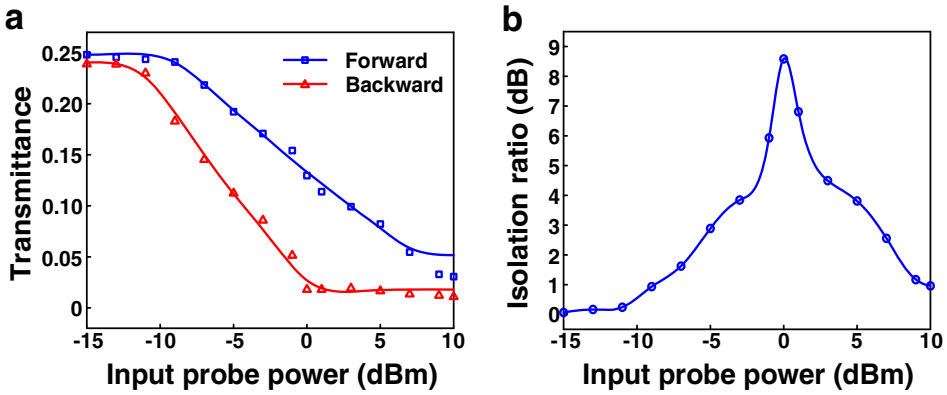

Fig. 5 Isolation performance. Experimental results of the isolation performance in the broken-PT-symmetric FP resonators. **a**. The transmittances of the probe signal entering the device in the forward (blue squares) and backward (red triangles) propagation directions, measured as a function of the probe power when the pumping power and the coupling strength are fixed. **b**. The isolation ratio as a function of the probe power.

on the probe power and the pumping power. Figure 5a shows the transmittances of the device for forward and backward transmission with a varying probe power from −15 to 10 dBm at a fixed the pumping power of 100 mW. At low probe power levels, the signal powers in FP2 are below the saturation threshold for both transmission directions, which leads to a linear input-output relation. In this case, gain saturation would not occur, and the nonreciprocity is weak. At high probe power levels, the signal powers in FP2 are beyond the saturation threshold for both transmission directions. In this case, the gain provided by EYDF is negligible for the probe signal entering the device from either direction, the system operates in the reciprocal regime. Strong nonreciprocity is observed at a probe power of 0 dBm, as shown in Fig. 5b. In this case, the signal power in FP2 reaches the saturation threshold only for the backward incident direction, because the probe power for the forward incident direction is attenuated in FP1 before it enters FP2. Thus, the backward-propagating light suffers from a lower gain due to the enhanced gain-saturation-induced nonlinearity compared with the forward-propagating light.

As a result, the unequal gains in the forward and backward propagating directions lead to a nonreciprocal response of the device. Note that an appropriate pumping power is also essential for the implementation of optical nonreciprocity in the device. A lower pumping power corresponds to a lower small-signal gain g' for the forward transmission, but the backward transmission is still strongly attenuated because of the gain-saturation-induced nonlinearity enhanced by broken PT symmetry, which leads to a weaker nonreciprocity. However, the nonreciprocity of this device with an excessive pumping power is still weak because it cannot be constructed as a PT symmetric system. The details on the quantification of gain and loss in each FP resonator are discussed in Supplementary Note 7.

The key to achieve optical nonreciprocity in the proposed all-fiber device was to use broken PT symmetry, by which the probe light entering the device from the gain section was highly saturated with less gain due to the strong confinement of the probe light in the gain FP resonator. For the probe light entering the device from the loss section, the probe signal was first attenuated at the loss section and then amplified at the gain section, leading to no or less gain saturation; therefore the overall gain for the second case is higher than that in the first case, and optical nonreciprocity was then achieved. The proposed all-fiber nonreciprocal device was fabricated, and its operation was experimentally demonstrated. Nonreciprocal light transmission with an isolation ratio of 8.58 dB at 1550 nm and a low insertion loss of 2.5 dB was experimentally demonstrated. By optimizing the design, the isolation ratio up to 33 dB could be achieved.

Conclusion

We have proposed and experimentally demonstrated an approach to implement an all-fiber nonreciprocal device using two mutually coupled PT-symmetric FP resonators. Thanks to the geometrical arrangement of the two FP resonators, PT symmetry of the system was achieved by controlling the pumping power of the FP resonators, to make the gain and the loss in the two FP resonators identical in magnitude. When the gain/loss coefficient was greater than the coupling coefficient, PT symmetry was broken, then the light in the gain FP resonator was highly confined, which was used to increase the gain-saturation nonlinearity, a key effect that leads to the optical nonreciprocity. The key advantages of the proposed device include all-fiber nature, which makes it possible to have the device integrated in an optical network without additional packaging. In addition, the device is all optically controlled and the isolation direction can be reversed by altering the direction of the pump light, which will increase its flexibility and can be potentially applied in a full duplex single-fiber optical link (see Supplementary Note 8). The bandwidth, due to the use of FP resonators was limited to few hundred of megahertz, which can be extended up to gigahertz by designing the FP resonators with lower Q-factors.

Method

Device fabrication. The device was fabricated by inscribing three FBGs to form two FP resonators in an EYDF using a phase mask which was illuminated by a 193-nm ArF excimer laser. The pulse energy and the repetition rate of the excimer laser were 110 mJ and 30 Hz, respectively. The phase-mask has a period of 1070.49 nm and a corresponding Bragg wavelength of 1552 nm. The reflectivity and bandwidth of the three FBGs are 94% and 0.2 nm, respectively. The lengths of the three FBGs and the two FP cavities are 4 mm and 10 mm, respectively. The device has a total length of 32 mm. The distance between adjacent gratings was controllable by moving the translational stage where the the phase mask was mounted during FBG fabrication process. The fiber used in the system is a commercial Er/Yb co-doped active fiber (EY305 from CorActive), which is a single mode fiber (SMF) and can only support one transverse mode. The core is Er/Yb co-doped silica glass and the core diameter is 8–10 μm. The cladding is silica glass and the diameter is 125 μm. The numerical aperture of the fiber is 0.18 and the mode field diameter at 1550 nm is 7 μm. The fiber has a cut-off wavelength of 1277 nm, which is less than the operating wavelength and the single-mode operating condition is satisfied. The peak absorption of the EYDF at 975 nm and 1535 nm are 1337 dB/m and 22 dB/m, respectively. The refractive index of the EYDF at 1550 nm is about 1.4485.

Data availability

All the data supporting the findings of this study are available from the corresponding authors upon request.

Code availability

The code used for the analyses will be made available upon e-mail request to the corresponding author.

Received: 27 September 2022; Accepted: 13 December 2022;
Published online: 23 December 2022

References

1. Jalas, D. et al. What is—and what is not—an optical isolator. *Nat. Photonics* **7**, 579–582 (2013).
2. Fujii, Y. High-isolation polarization-independent optical circulator. *J. Lightwave Technol.* **9**, 1238–1243 (1991).
3. Aleahmad, P., Khajavikhan, M., Christodoulides, D. & LiKamWa, P. Integrated multi-port circulators for unidirectional optical information transport. *Sci. Rep.* **7**, 2129 (2017).
4. Petermann, K. External optical feedback phenomena in semiconductor lasers. *IEEE J. Sel. Top. Quantum Electron* **1**, 480–489 (1995).
5. Bi, L. et al. On-chip optical isolation in monolithically integrated non-reciprocal optical resonators. *Nat. Photonics* **5**, 758–762 (2011).
6. Yan, W. et al. Waveguide-integrated high-performance magneto-optical isolators and circulators on silicon nitride platforms. *Optica* **7**, 1555–1562 (2020).
7. Stadler, B. J. & Mizumoto, T. Integrated magneto-optical materials and isolators: a review. *IEEE Photon. J.* **6**, 1–15 (2013).
8. Zhang, Y. et al. Monolithic integration of broadband optical isolators for polarization-diverse silicon photonics. *Optica* **6**, 473–478 (2019).
9. Zhang, C., Dulal, P., Stadler, B. J. & Hutchings, D. C. Monolithically-integrated TE-mode 1D silicon-on-insulator isolators using seedlayer-free garnet. *Sci. Rep.* **7**, 5820 (2017).
10. Tien, M.-C., Mizumoto, T., Pintus, P., Kromer, H. & Bowers, J. E. Silicon ring isolators with bonded nonreciprocal magneto-optic garnets. *Opt. Express* **19**, 11740–11745 (2011).
11. Kim, S., Sohn, D. B., Peterson, C. W. & Bahl, G. On-chip optical non-reciprocity through a synthetic Hall effect for photons. *APL Photonics* **6**, 011301 (2021).
12. Sun, L., Jiang, S., Zuegel, J. & Marciante, J. All-fiber optical isolator based on Faraday rotation in highly terbium-doped fiber. *Opt. Lett.* **35**, 706–708 (2010).
13. Wolfe, R., Wang, W.-K., DiGiovanni, D. & Vengsarkar, A. All-fiber magneto-optic isolator based on the nonreciprocal phase shift in asymmetric fiber. *Opt. Lett.* **20**, 1740–1742 (1995).
14. Sounas, D. L. & Alù, A. Non-reciprocal photonics based on time modulation. *Nat. Photonics* **11**, 774–783 (2017).
15. Estep, N. A., Sounas, D. L., Soric, J. & Alù, A. Magnetic-free non-reciprocity and isolation based on parametrically modulated coupled-resonator loops. *Nat. Phys.* **10**, 923–927 (2014).
16. Lira, H., Yu, Z., Fan, S. & Lipson, M. Electrically driven nonreciprocity induced by interband photonic transition on a silicon chip. *Phys. Rev. Lett.* **109**, 033901 (2012).
17. Kittlaus, E. A. et al. Electrically driven acousto-optics and broadband non-reciprocity in silicon photonics. *Nat. Photonics* **15**, 43–52 (2021).
18. Tian, H. et al. Magnetic-free silicon nitride integrated optical isolator. *Nat. Photonics* **15**, 828–836 (2021).
19. Fan, L. et al. An all-silicon passive optical diode. *Science* **335**, 447–450 (2012).
20. Hua, S. et al. Demonstration of a chip-based optical isolator with parametric amplification. *Nat. Commun.* **7**, 13657 (2016).
21. Krause, M., Renner, H. & Brinkmeyer, E. Optical isolation in silicon waveguides based on nonreciprocal Raman amplification. *Electron. Lett.* **44**, 691–693 (2008).
22. Dong, C.-H. et al. Brillouin-scattering-induced transparency and non-reciprocal light storage. *Nat. Commun.* **6**, 6193 (2015).
23. Kim, J., Kuzyk, M. C., Han, K., Wang, H. & Bahl, G. Non-reciprocal Brillouin scattering induced transparency. *Nat. Phys.* **11**, 275–280 (2015).
24. Poulton, C. G. et al. Design for broadband on-chip isolator using stimulated Brillouin scattering in dispersion-engineered chalcogenide waveguides. *Opt. Express* **20**, 21235–21246 (2012).
25. Ma, J. et al. Chip-Based Optical Isolator and Nonreciprocal Parity-Time Symmetry Induced by Stimulated Brillouin Scattering. *Laser Photonics Rev.* **14**, 1900278 (2020).
26. Grigoriev, V. & Biancalana, F. Nonreciprocal switching thresholds in coupled nonlinear microcavities. *Opt. Lett.* **36**, 2131–2133 (2011).
27. Del Bino, L. et al. Microresonator isolators and circulators based on the intrinsic nonreciprocity of the Kerr effect. *Optica* **5**, 279–282 (2018).
28. Shen, Z. et al. Experimental realization of optomechanically induced non-reciprocity. *Nat. Photonics* **10**, 657–661 (2016).
29. Ruesink, F., Miri, M.-A., Alu, A. & Verhagen, E. Nonreciprocity and magnetic-free isolation based on optomechanical interactions. *Nat. Commun.* **7**, 13662 (2016).
30. Fang, K. et al. Generalized non-reciprocity in an optomechanical circuit via synthetic magnetism and reservoir engineering. *Nat. Phys.* **13**, 465–471 (2017).
31. Shen, Z. et al. Reconfigurable optomechanical circulator and directional amplifier. *Nat. Commun.* **9**, 1797 (2018).
32. Ruesink, F., Mathew, J. P., Miri, M.-A., Alù, A. & Verhagen, E. Optical circulation in a multimode optomechanical resonator. *Nat. Commun.* **9**, 1798 (2018).
33. Hafezi, M. & Rabl, P. Optomechanically induced non-reciprocity in microring resonators. *Opt. Express* **20**, 7672–7684 (2012).
34. Chang, L. et al. Parity–time symmetry and variable optical isolation in active–passive-coupled microresonators. *Nat. Photonics* **8**, 524–529 (2014).
35. Peng, B. et al. Parity–time-symmetric whispering-gallery microcavities. *Nat. Phys.* **10**, 394–398 (2014).
36. Bender, C. M. & Boettcher, S. Real spectra in non-Hermitian Hamiltonians having P T symmetry. *Phys. Rev. Lett.* **80**, 5243 (1998).
37. El-Ganainy, R. et al. Non-Hermitian physics and PT symmetry. *Nat. Phys.* **14**, 11–19 (2018).
38. Schindler, J., Li, A., Zheng, M. C., Ellis, F. M. & Kottos, T. Experimental study of active LRC circuits with PT symmetries. *Phys. Rev. A* **84**, 040101 (2011).
39. Shi, C. et al. Accessing the exceptional points of parity-time symmetric acoustics. *Nat. Commun.* **7**, 11110 (2016).
40. Aurégan, Y. & Pagneux, V. P T-symmetric scattering in flow duct acoustics. *Phys. Rev. Lett.* **118**, 174301 (2017).
41. Zhu, X., Ramezani, H., Shi, C., Zhu, J. & Zhang, X. P t-symmetric acoustics. *Phys. Rev. X* **4**, 031042 (2014).
42. Fleury, R., Sounas, D. & Alu, A. An invisible acoustic sensor based on parity-time symmetry. *Nat. Commun.* **6**, 5905 (2015).
43. Zhang, J. et al. Giant nonlinearity via breaking parity-time symmetry: A route to low-threshold phonon diodes. *Phys. Rev. B* **92**, 115407 (2015).
44. Shao, L. et al. Non-reciprocal transmission of microwave acoustic waves in nonlinear parity–time symmetric resonators. *Nat. Electron.* **3**, 267–272 (2020).
45. Rüter, C. E. et al. Observation of parity–time symmetry in optics. *Nat. Phys.* **6**, 192–195 (2010).
46. Guo, A. et al. Observation of P T-symmetry breaking in complex optical potentials. *Phys. Rev. Lett.* **103**, 093902 (2009).
47. Regensburger, A. et al. Parity–time synthetic photonic lattices. *Nature* **488**, 167–171 (2012).
48. Feng, L. et al. Experimental demonstration of a unidirectional reflectionless parity-time metamaterial at optical frequencies. *Nat. Mater.* **12**, 108–113 (2013).
49. Feng, L., Wong, Z. J., Ma, R.-M., Wang, Y. & Zhang, X. Single-mode laser by parity-time symmetry breaking. *Science* **346**, 972–975 (2014).
50. Hodaei, H., Miri, M.-A., Heinrich, M., Christodoulides, D. N. & Khajavikhan, M. Parity-time–symmetric microring lasers. *Science* **346**, 975–978 (2014).
51. Li, L. et al. Polarimetric parity-time symmetry in a photonic system. *Light Sci. Appl.* **9**, 169 (2020).
52. Lax, M., Agrawal, G., Belic, M., Coffey, B. & Louisell, W. Electromagnetic-field distribution in loaded unstable resonators. *J. Opt. Soc. Am. A* **2**, 731–742 (1985).

Acknowledgements

This work was supported by the National Key R&D Program of China (2021YFB2800804), National Natural Science Foundation of China (61860206002) and the Guangdong Province Key Field R&D Program Project (2020B0101110002).

Author contributions

J.Z. and J.Y. conceived the idea; J.Z. designed the experiment and wrote the paper; Z.L. conducted the theoretical simulations, device fabrication and testing, and wrote the paper; L.L. and B.L. contributed to device fabrication and testing; J.Y. analyzed the data and wrote the paper; Y.Z. wrote the paper.

Competing interests

The authors declare no competing interests.

Additional information

Supplementary information The online version contains supplementary material available at https://doi.org/10.1038/s42005-022-01120-w.

Correspondence and requests for materials should be addressed to Jiejun Zhang or Jianping Yao.

Peer review information *Communications Physics* thanks the anonymous reviewers for their contribution to the peer review of this work. Peer reviewer reports are available.